ADVANCED MATERIALS

Supporting Information

for *Adv. Mater.,* DOI: 10.1002/adma.202200401

Long-Cycling Sulfide-Based All-Solid-State Batteries Enabled by Electrochemo-Mechanically Stable Electrodes

*Daxian Cao, Xiao Sun, Yejing Li, Alexander Anderson, Wenquan Lu, and Hongli Zhu**

Supplementary Materials

Long-Cycling Sulfide-Based All-Solid-State Batteries Enabled by Electrochemo-Mechanically Stable Electrodes

Daxian Cao,[1] Xiao Sun,[1] Yejing Li,[2] Alexander Anderson,[1] Wenquan Lu,[2] Hongli Zhu[1]*

[1]Department of Mechanical and Industrial Engineering, Northeastern University, Boston, MA, 02115, USA

[2]Chemical Science and Engineering Division, Argonne National Laboratory, Lemont, IL, 60439, USA

***Corresponding author.** h.zhu@neu.edu*

This PDF file includes:

Figs. S1 to S26
Tables S1 to S2
References (S1 to S5)

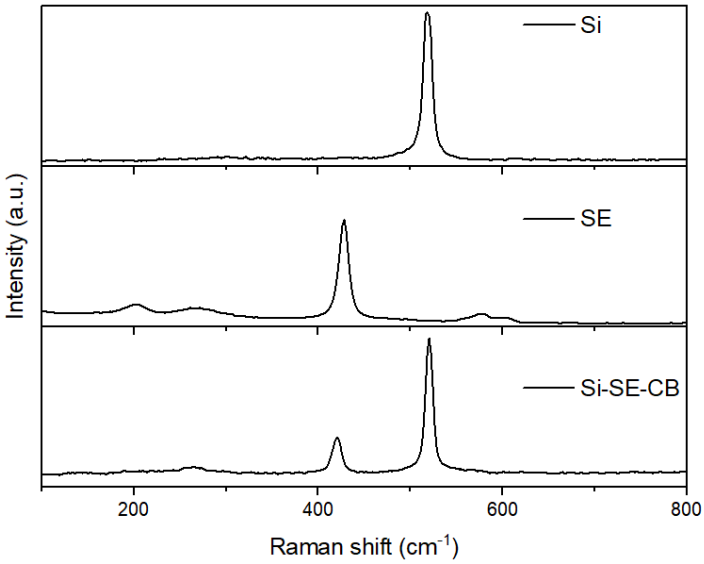

Figure S1. Raman spectra of Si composite anode in comparison with pure Si and SE.

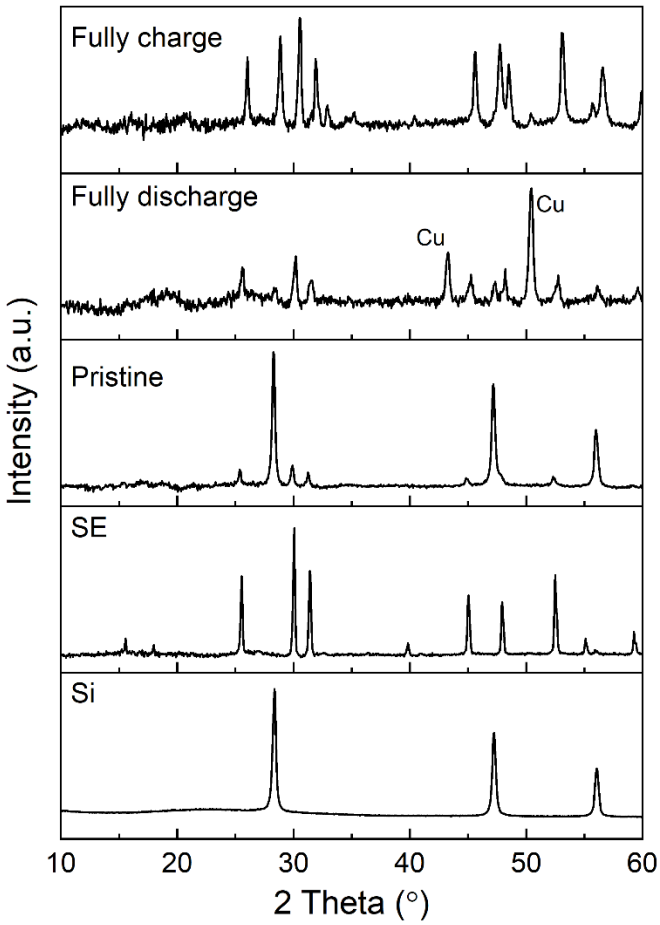

Figure S2. XRD spectra of Si composite anode at various charge and discharge state at first cycle.

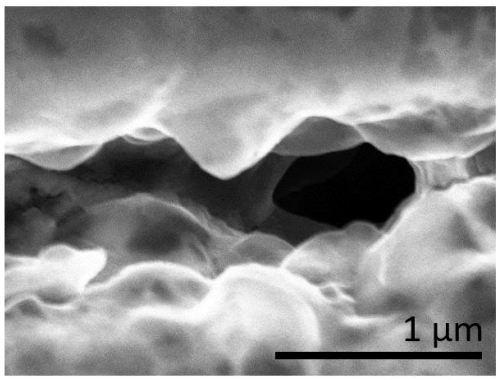

Figure S3. Magnified top view SEM image of the crack of Si anode after cycling.

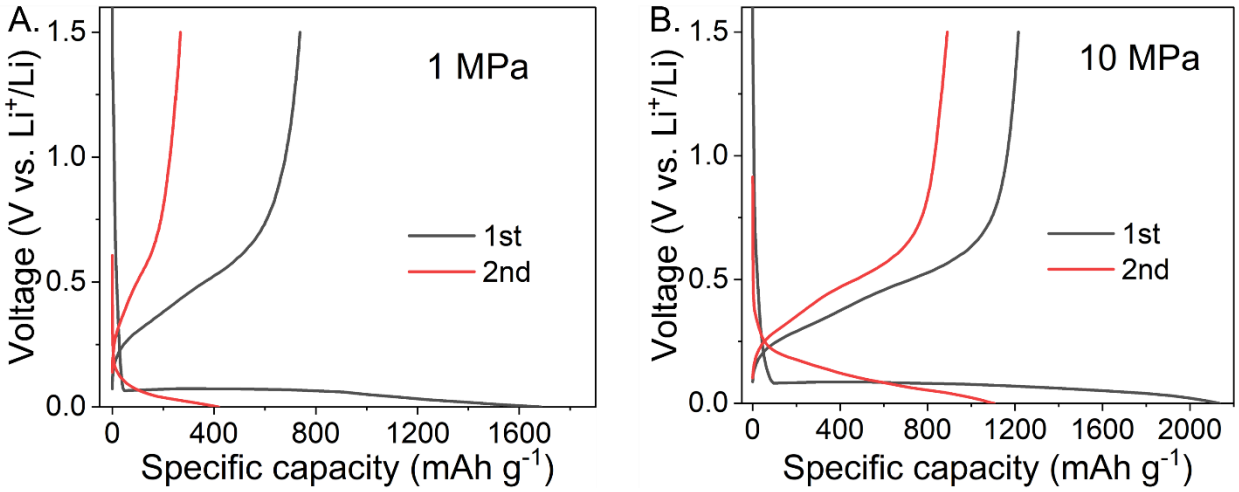

Figure S4. Galvanostatic charge/discharge profiles of the Si half cells cycled at the external pressures of (A) 1 MPa and (B) 10 MPa.

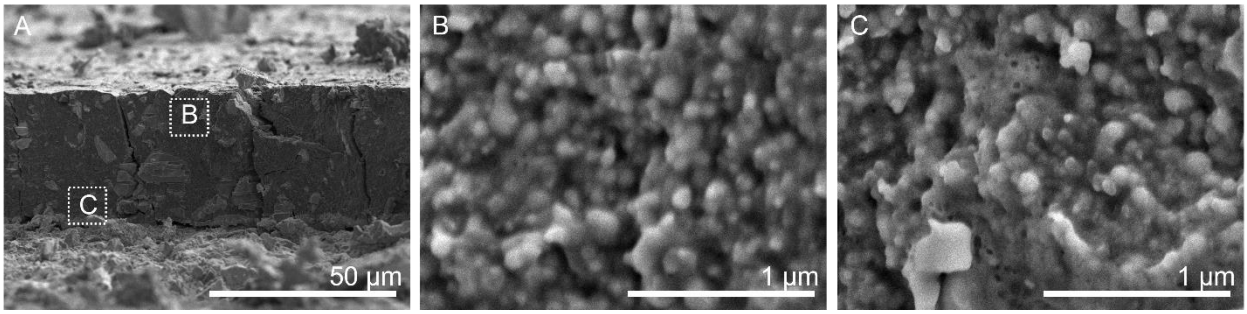

Figure S5. (A) Cross-section image of Si composite anode after cycling at the pressure of 10 MPa. (B) Zooming in image of the region near the current collector. (C) Zooming in image of the region near the SE layer.

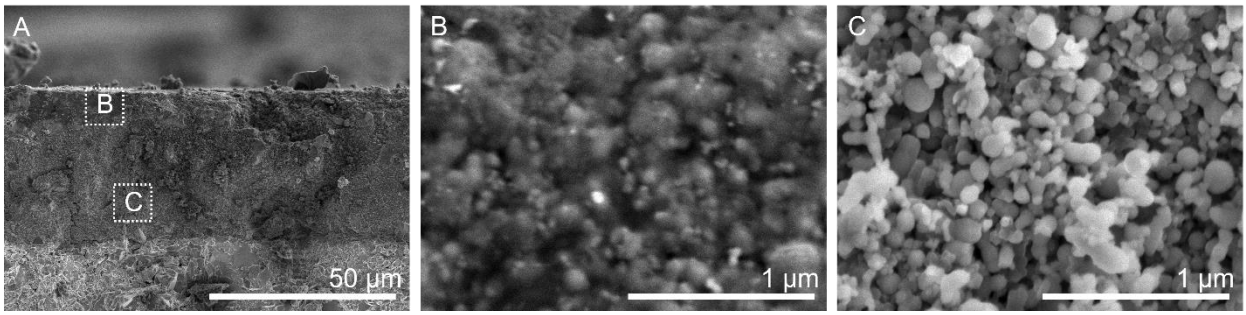

Figure S6. (A) Cross-section image of Si composite anode after cycling at the pressure of 1 MPa. (B) Zooming in image of the region near the current collector. (C) Zooming in image of the region near the SE layer.

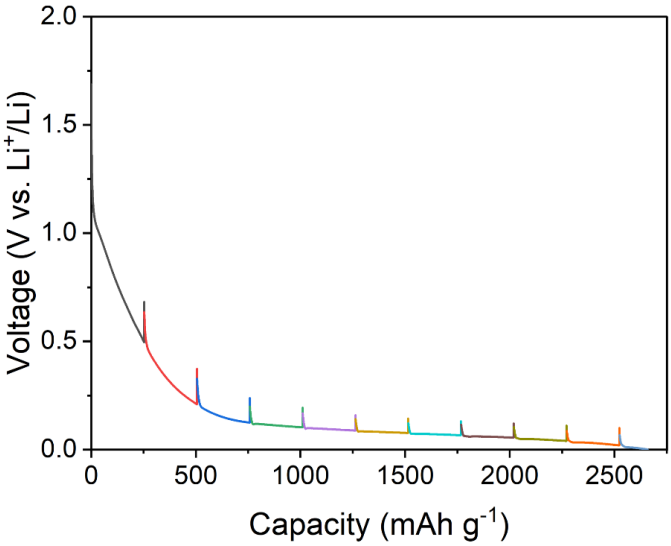

Figure S7. Discharge profile of the half cell at the current density of 0.25 mA cm^{-2}. The EIS was measured every hour discharge. A 30 min interval was applied before the EIS test.

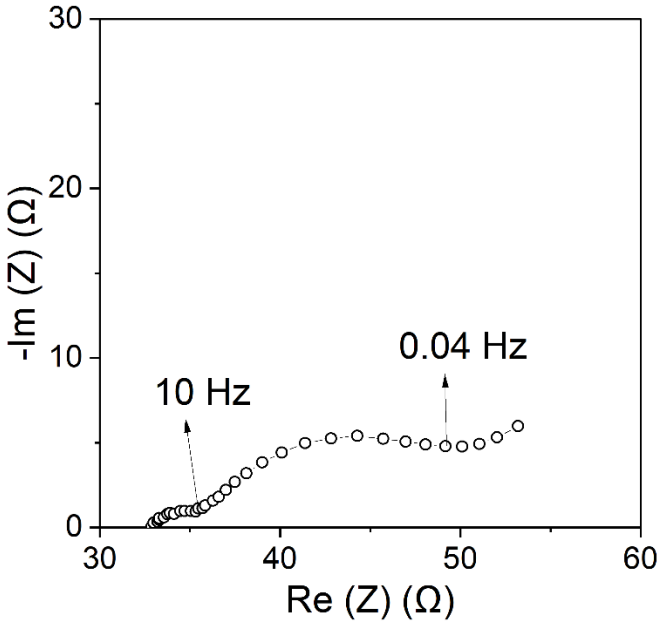

Figure S8. Nyquist plot of InLi|SE|InLi symmetric cell.

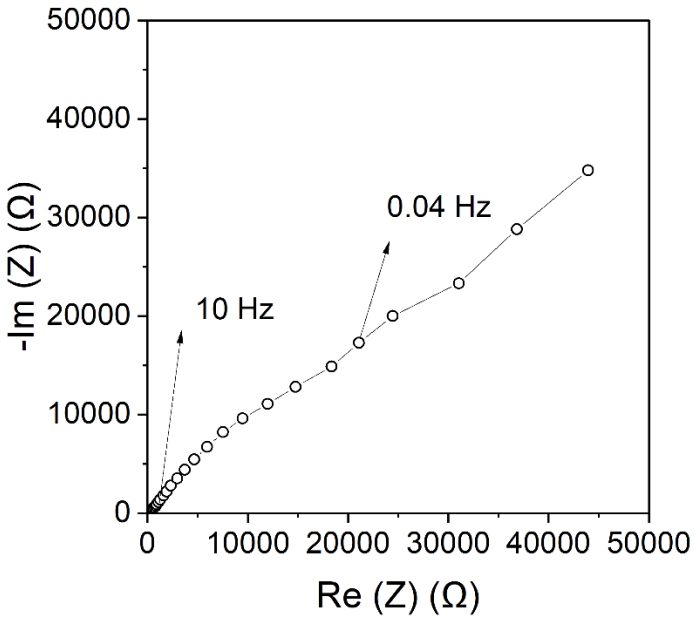

Figure S9. Nyquist plot of Si-SE-CB|SE|Si-SE-CB symmetric cell.

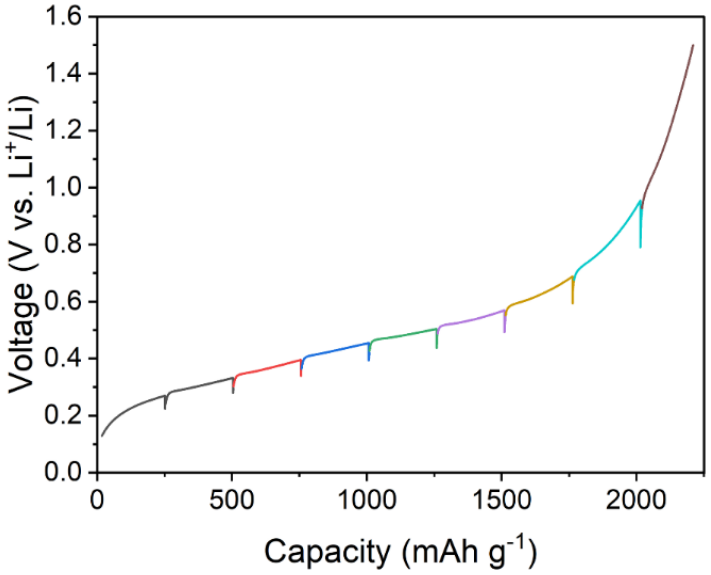

Figure S10. Charge profile of the half cell at the current density of 0.25 mA cm^{-2}. The EIS was measured every hour discharge. A 30 min interval was applied before the EIS test.

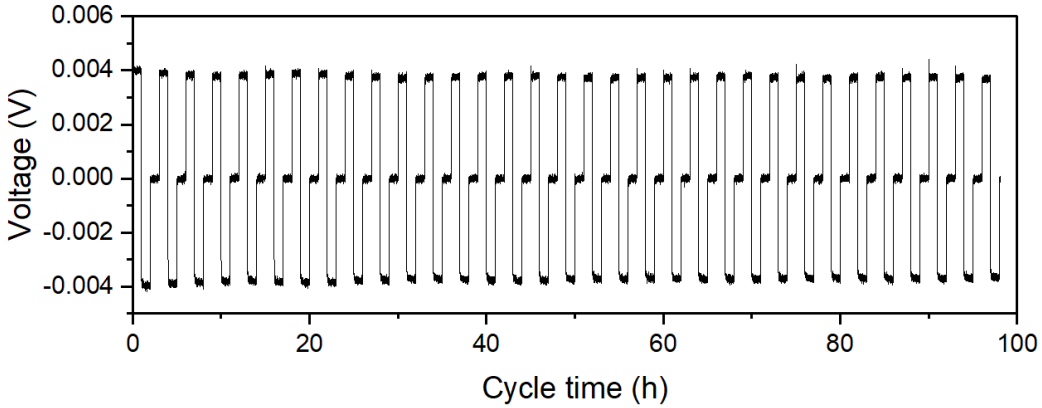

Figure S11. Following cycling performance of Li|SE|Li symmetric cell. Though the Nyquist plot was not a typical behavior of short circuit, the cell was in a soft short circuit.

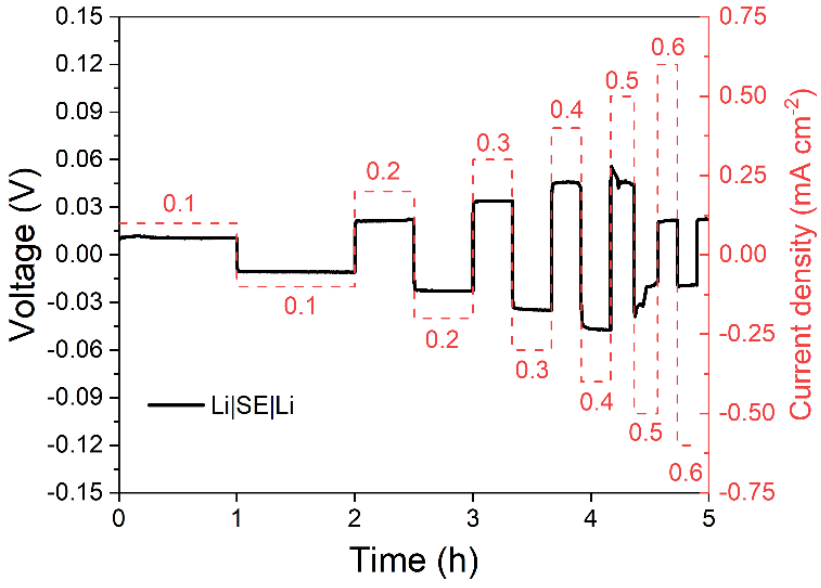

Figure S12. Critical current density measurement of Li metal anode.

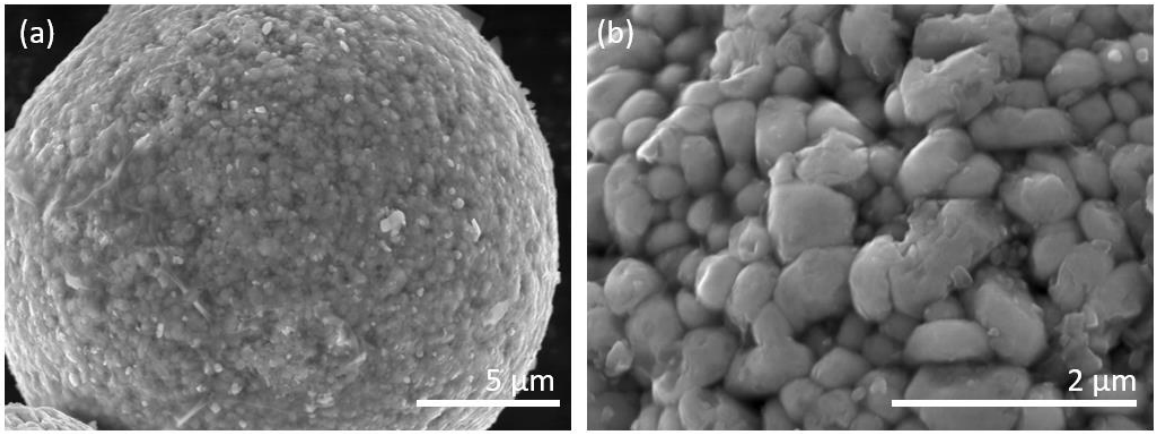

Figure S13. SEM images of Li_2SiO_x coated polycrystalline NMC 811 at (a) low and (b) high magnificence.

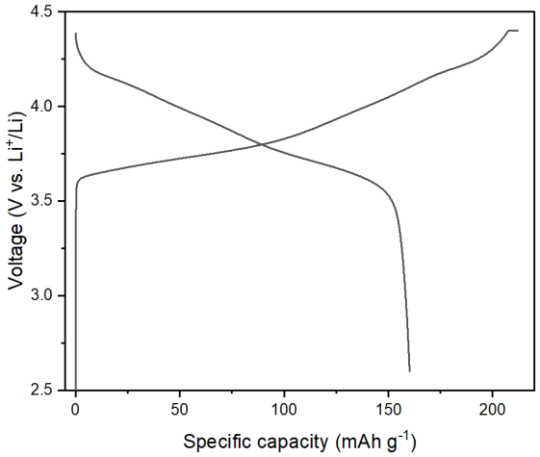

Figure S14. Charge/discharge profile of the ASLBs using bare single crystal NMC 811 as cathode active material.

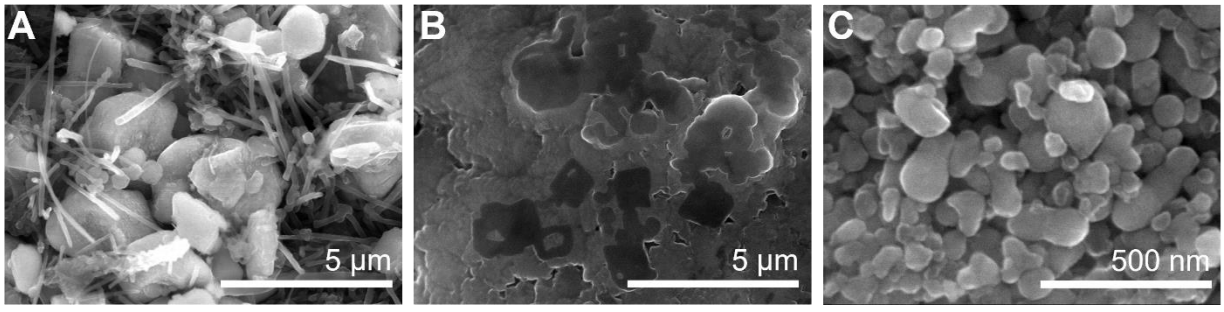

Figure S15. SEM images of the (A) composite cathode, (B) SE, and (C) composite anode in the full cell.

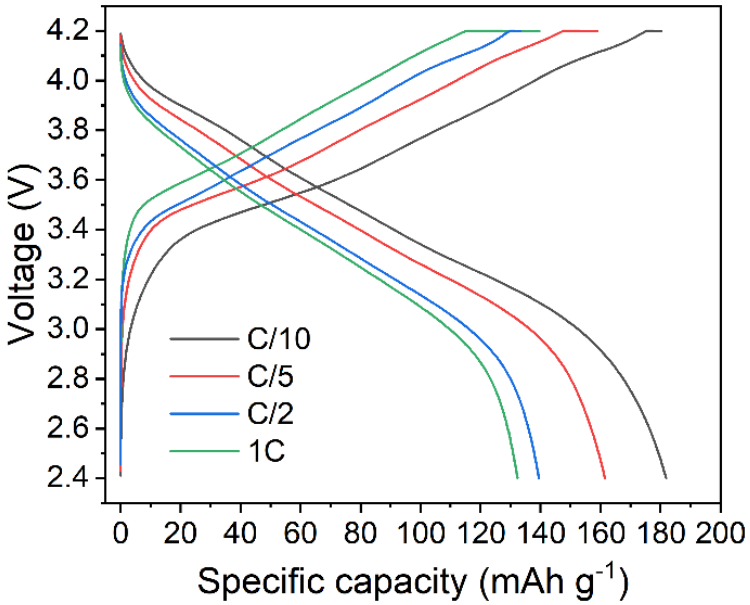

Figure S16. The galvanostatic charge and discharge profile of full cell with cathode mass loading of 10 mg cm^{-2} at first cycle at the rate of C/10, C/5, C/2, and 1C.

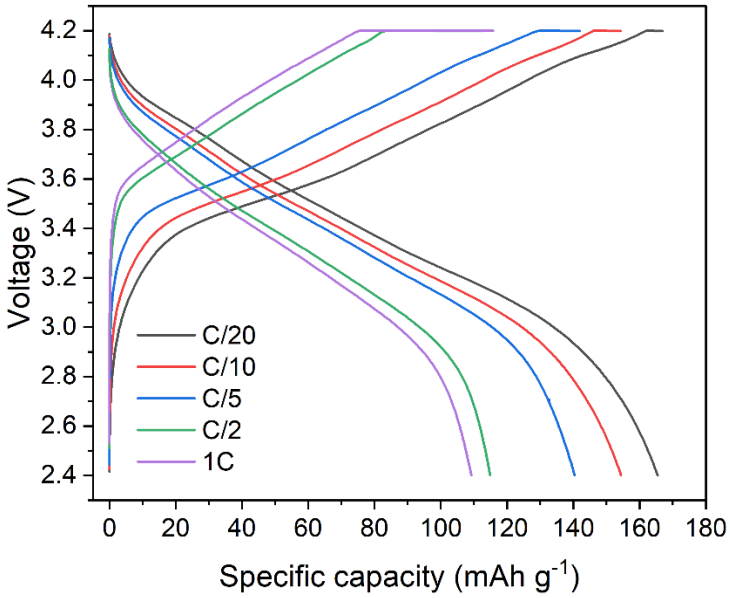

Figure S17. The galvanostatic charge and discharge profile of full cell with cathode mass loading of 20 mg cm^{-2} at first cycle at the rate of C/10, C/5, C/2, and 1C.

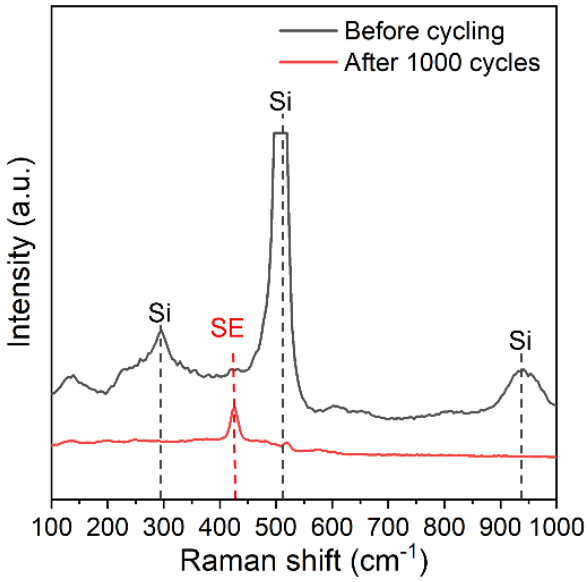

Figure S18. Raman spectra of the Si composite anode before and after 1000 cycles.

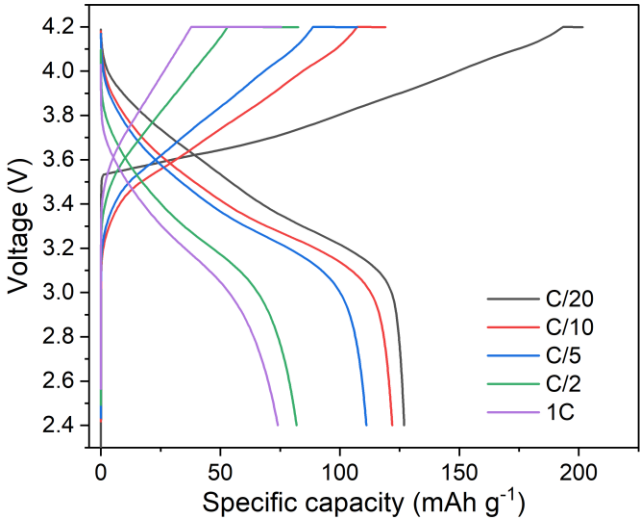

Figure S19. Charge/discharge profiles of the full cell using pure Si as anode.

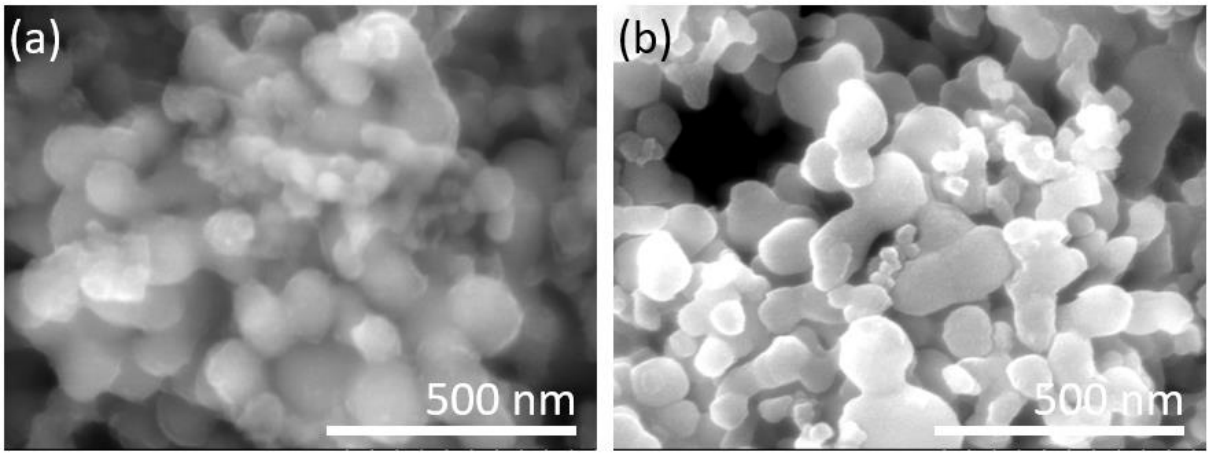

Figure S20. SEM images of (a) C@Si and (b) LPS@Si.

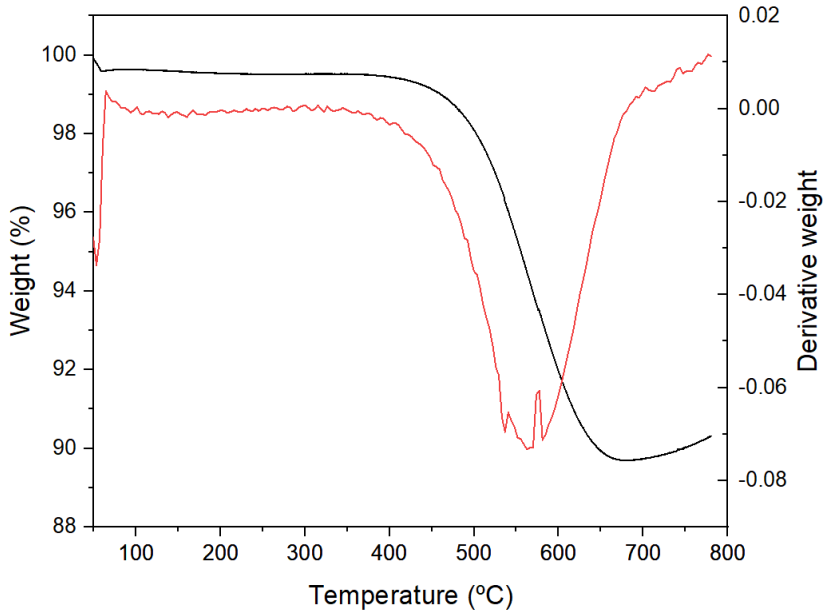

Figure S21. Thermo gravimetric analysis of the C@Si.

The weight loss before 650 ºC was mainly caused by the burning of carbon coating in the air, while the slightly weight rise was attributed to the oxidization of Si at high temperature.

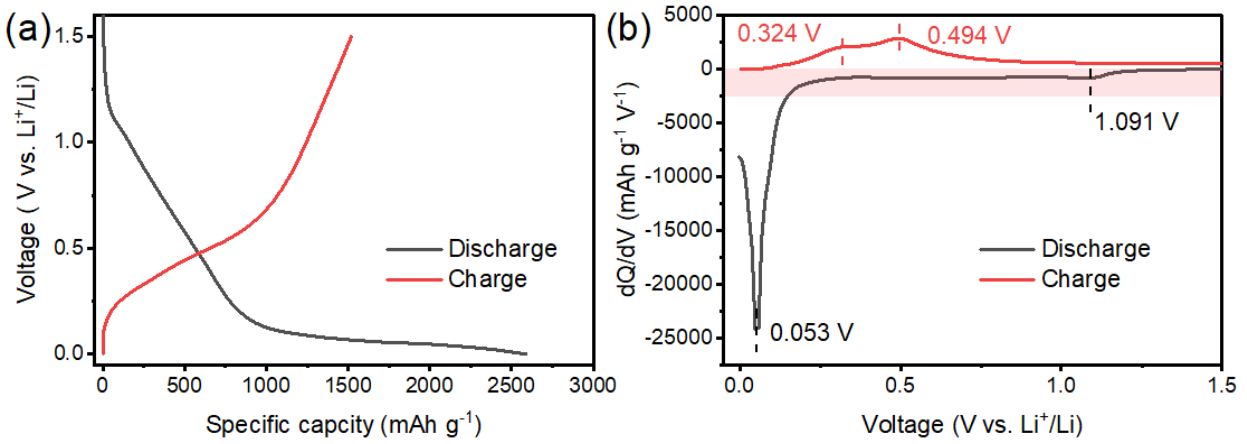

Figure S22. Half cell performance of C@Si-SE. (a) Galvanostatic charge/discharge profiles and (b) corresponding dQ/dV profiles of the half cell at first cycle.

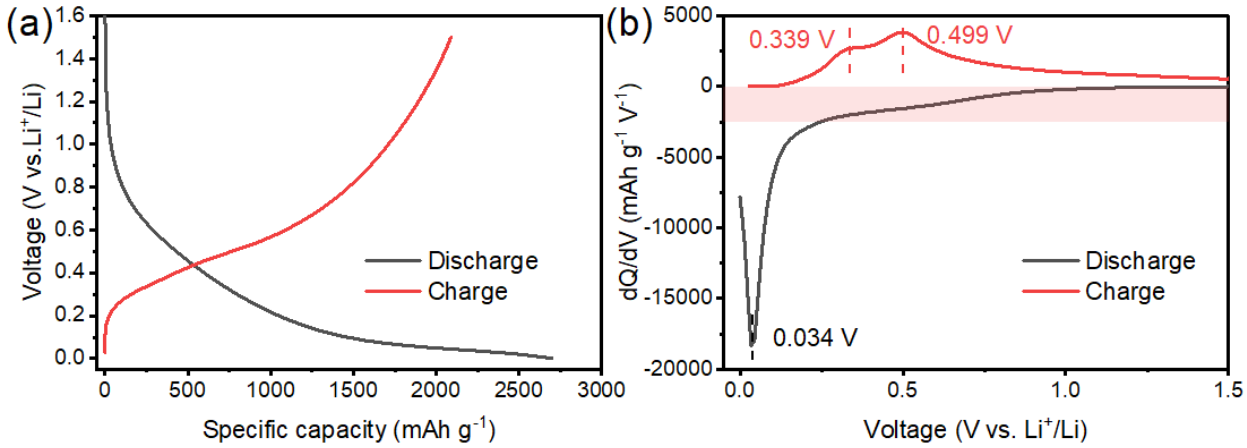

Figure S23. Half cell performance of LPS@Si-SE-CB. (a) Galvanostatic charge/discharge profiles and (b) corresponding dQ/dV profiles of the half cell at first cycle.

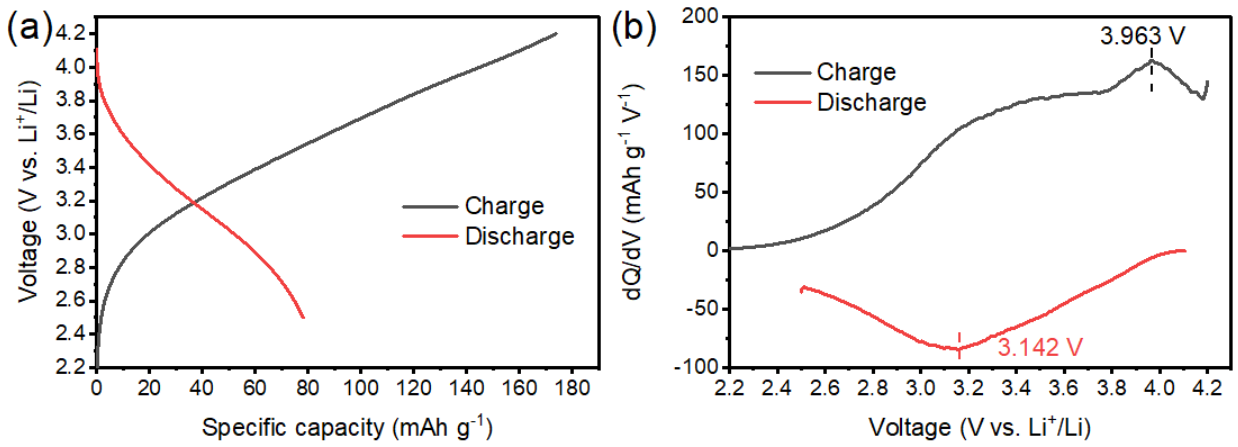

Figure S24. Full cell performance of C@Si-SE. (a) Galvanostatic charge/discharge profiles and (b) corresponding dQ/dV profiles of the full cell at first cycle.

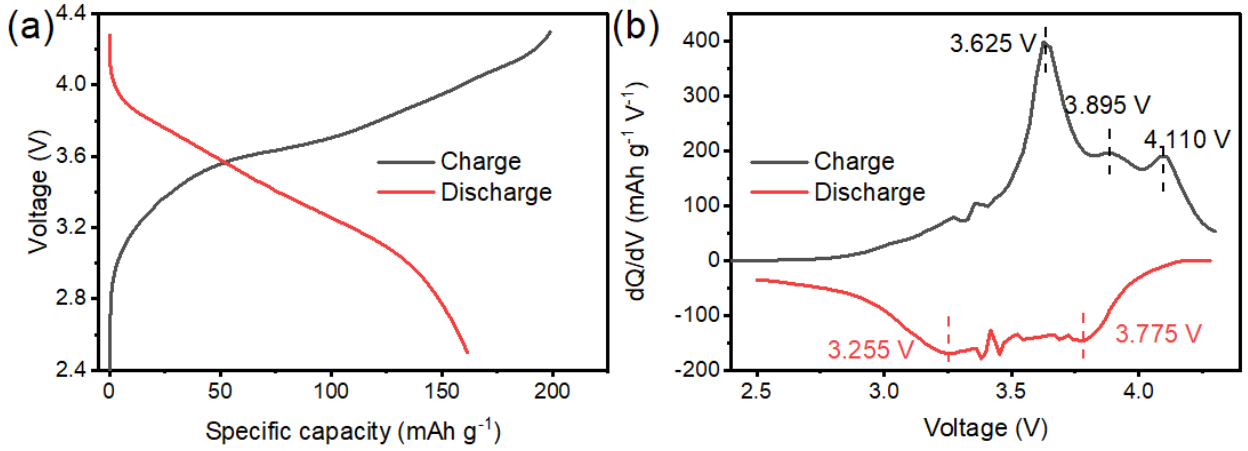

Figure S25. Full cell performance of LPS@Si-SE-CB. (a) Galvanostatic charge/discharge profiles and (b) corresponding dQ/dV profiles of the full cell at first cycle.

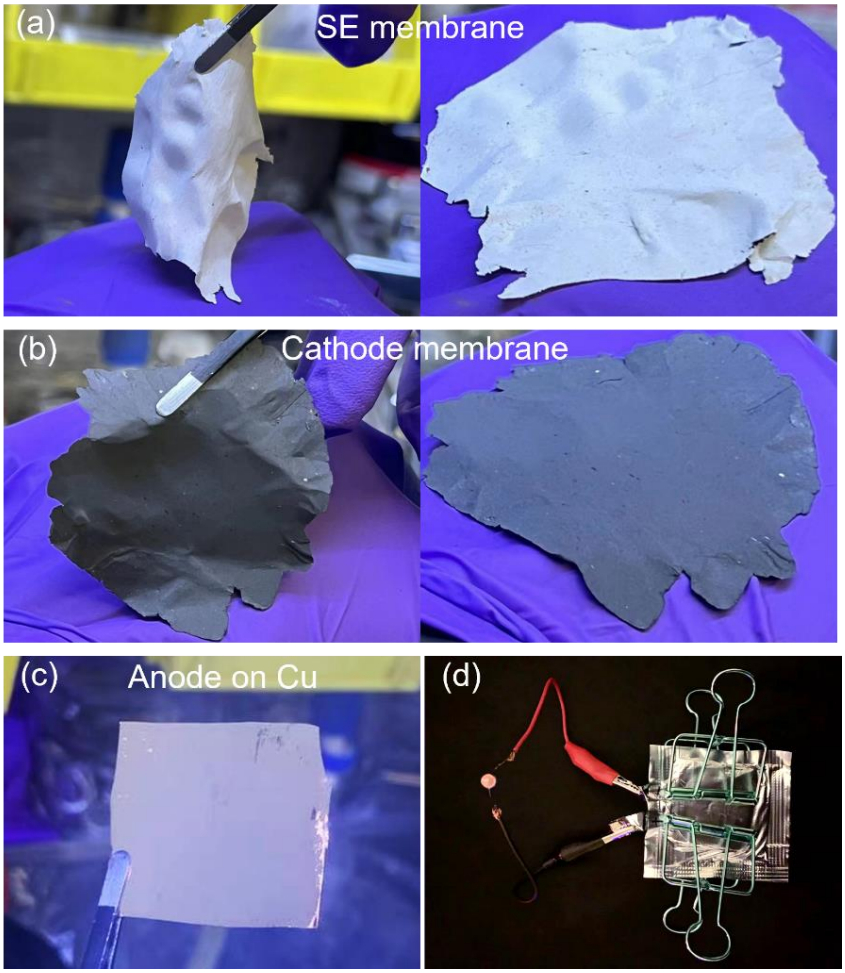

Figure S26. Pouch cell assembly. Photos of (a) SE and (b) cathode membranes. (c) Photo of Si anode cast on Cu foil. (d) Photo of pouch cell lightening a bulb.

Table 1. Estimated energy densities of ASLBs using Si anode and Li metal anode.

Gravimetric energy density (Wh kg^{-1})	Volumetric energy density (Wh L^{-1})	Average voltage (V)	Cathode	Press density of cathode (g cm^{-3})	Reversible capacity (mAh g^{-1})	Initial Coulombic efficiency (%)	Mass (mg)	Ratio of CAM (%)	Anode	N/P	Press density of anode (g cm^{-3})	Reversible capacity (mAh g^{-1})	Initial coulombic efficiency (%)
964.7	355.7	3.4	NMC 811	3.5	200	90	25	80	Si	1.05	1.91	2600	85
928.1	409.6	3.8	NMC 811	3.5	200	90	25	80	Li metal	2	0.53	3800	100

Table 2. Cell-level energy densities of ASLBs in comparison with reported work. The highlighted values are estimated based on the description of experiment.

Mass of AAM (mg cm^{-2})	Mass of anode (mg cm^{-2})	Mass of SE (mg cm^{-2})	Mass of CAM (mg cm^{-2})	Mass of cathode (mg cm^{-2})	Current density (mA cm^{-2})	Average voltage (V)	Specific capacity (mAh g^{-1})	Cell-level energy density (Wh kg^{-1})	
0.95	1.59	7.93	7.93	9.92	0.079	3.4	188	260.89	This work
					0.158	3.39	178	246.29	
					0.316	3.39	162	224.16	
					0.79	3.38	143	197.28	
					1.58	3.34	130	177.22	
1.90	3.17	7.93	15.87	19.84	0.158	3.37	165	285.15	
					0.316	3.35	154	264.56	
					0.632	3.34	142	243.95	
					1.58	3.33	111	189.55	
					3.16	3.29	105	177.15	
0.60	0.86	113.07	5.65	7.54	0.056	3.4	155	24.52	Ref. S1[1]
1.46	2.68	7.6	9.68	22.68	0.15	3.4	132	212.16	Ref. S2[2]
					0.3	3.4	100	160.73	
					0.75	3.4	88	112.51	
					1.5	3.4	65	61.08	
					3	3.4	32	24.11	
0.46	0.92	113.07	10	20.00	0.14	3.5	104	27.17	Ref. S3[3]
					0.28	3.5	93	24.29	
1.40	2.55	15.29	14.10	17.62	0.15	3.4	132	178.46	Ref. S4[4]
					0.3	3.35	110	146.53	
					0.75	3.3	88	115.47	
					1.5	3.1	65	80.12	
					3	3	35	41.75	
1.00	1.00	113.07	9.58	11.31	0.15	3.4	203	52.75	Ref. S5[5]
					0.45	3.4	180	46.77	
					0.75	3.39	170	44.04	
					1.6	3.3	160	40.35	

[1] N. A. Dunlap, J. Kim, H. Guthery, C.-S. Jiang, I. Morrissey, C. R. Stoldt, K. H. Oh, M. Al-Jassim, S.-H. Lee, Journal of The Electrochemical Society 2020, 167, 060522.

[2] M. Yamamoto, Y. Terauchi, A. Sakuda, M. Takahashi, Journal of Power Sources 2018, 402, 506.

[3] D. H. Kim, H. A. Lee, Y. B. Song, J. W. Park, S.-M. Lee, Y. S. Jung, Journal of Power Sources 2019, 426, 143.

[4] M. Yamamoto, Y. Terauchi, A. Sakuda, A. Kato, M. Takahashi, Journal of Power Sources 2020, 473, 228595.

[5] S. Cangaz, F. Hippauf, F. S. Reuter, S. Doerfler, T. Abendroth, H. Althues, S. Kaskel, Advanced Energy Materials 2020, 10, 2001320.